Atmospheric Environment 42 (2008) 7988–7996

Contents lists available at ScienceDirect

Atmospheric Environment

journal homepage: www.elsevier.com/locate/atmosenv

Reactive and particulate mercury in the Asian marine boundary layer

Duli Chand [a,b,*], Daniel Jaffe [a,b], Eric Prestbo [c], Philip C. Swartzendruber [a,b], William Hafner [a], Peter Weiss-Penzias [d], Shungo Kato [e], Akinori Takami [f], Shiro Hatakeyama [f], Yoshizumi Kajii [e]

[a] University of Washington-Bothell, 18115 Campus Way NE, Bothell, WA 98011, USA
[b] Department of Atmospheric Sciences, University of Washington, Seattle, WA, USA
[c] Frontier Geosciences, 414 Pontius Avenue N., Seattle, WA 98109, USA
[d] Department of Environmental Toxicology, University of California, 1156 High Street, Santa Cruz, CA 95060, USA
[e] Applied Chemistry, Faculty of Engineering, Tokyo Metropolitan University, Tokyo, Japan
[f] Atmospheric Environmental Division, National Institute of Environmental Studies, Tsukuba, Japan

ARTICLE INFO

Article history:
Received 17 October 2007
Received in revised form 20 June 2008
Accepted 24 June 2008

Keywords:
Mercury
Pollution
Transport
Particulate
Reactive-mercury
Speciated-mercury

ABSTRACT

The variability of atmospheric mercury in elemental, reactive, and particulate forms has been studied at a remote site (Cape Hedo Observatory, CHO) at Okinawa Island (Japan) March 23 to May 2, 2004, downwind of the major Asian source regions. Under prevailing meteorological conditions, episodes of higher levels of atmospheric mercury and other atmospheric species are observed at CHO. The mean ($\pm 1\sigma$) concentrations of gaseous elemental mercury (GEM), reactive gaseous mercury (RGM) and particulate-bound mercury (PHg) are 2.04 ± 0.38 ng m^{-3}, 4.5 ± 5.4 pg m^{-3} and 3.0 ± 2.5 pg m^{-3}, respectively. In Asian outflow the combined contribution of RGM and PHg constitutes less than 1% of the GEM in the boundary layer, which indicates that most mercury export in the marine boundary layer is due to the GEM form, and direct outflow of RGM and PHg is very low. While the data from Okinawa suggest minimal export of RGM and PHg, this does not preclude greater export of these species at higher elevations. Based on the correlations of PHg and submicron aerosol mass (SAM), we found a ΔPHg/ΔSAM ratio of 0.20 μg g^{-1} ($R = 0.58$, $p < 0.01$), which we believe to be characteristic of East Asian industrial aerosols during outflow. A diurnal variation is observed in RGM with a peak near noon. Using a rate constant of 9×10^{-14} cm^3 molecule^{-1} s^{-1} for the OH oxidation rate (Sommar, J., Gardfeldt, K., Stromberg, D., Feng, X., 2001. A kinetic study of the gas phase reaction between the hydroxyl radical and atomic mercury. Atmospheric Environment 35, 3049–3054; Pal, B., Ariya, P.A., 2004a. Gas-phase HO center dot-initiated reactions of elemental mercury: kinetics, product studies, and atmospheric implications. Environmental Science and Technology 38 (21), 5555–5566.) and a typical OH concentration of $1–5 \times 10^6$ cm^{-3} would result in RGM production rates of 0.6–3.0 pg m^{-3} h^{-1}. Although OH may not be the sole oxidant, this is consistent with the observed change in concentration during daytime of 1.4 ± 1.5 pg m^{-3} h^{-1}. A significant correlation is found between GEM and CO; GEM and SAM; and PHg and SAM. Lower ΔSAM/ΔCO and ΔGEM/ΔCO are observed for transport events with rainfall and for air parcels remaining in the mixed layer. Back trajectory analysis along with the correlation study suggests that the air from China has a higher GEM concentration compared to the air coming from southern Japan.

* Corresponding author. University of Washington-Bothell, 18115 Campus Way NE, Bothell, WA 98011, USA. Fax: +1 206 685 9302.
E-mail address: duli@u.washington.edu (D. Chand).

1352-2310/$ – see front matter © 2008 Elsevier Ltd. All rights reserved.
doi:10.1016/j.atmosenv.2008.06.048

1. Introduction

Mercury is an atmospheric pollutant with a complex biogeochemical cycle (Schroeder and Munthe, 1998). Atmospheric mercury exists in three operationally defined forms: gaseous elemental mercury (GEM), divalent reactive gaseous mercury (RGM) and particulate mercury (PHg). The transport and fate of atmospheric mercury are a subject of much interest primarily for reasons of human health. Mercury is a neurotoxin and some mercury compounds such as methyl mercury have a high rate of bio-accumulation through the food chain (Lipfert et al., 2005 and references therein). Because of its long lifetime, long-range transport of GEM at the inter-continental scale has been observed (Carpi, 1997; Jaffe et al., 2005; Weiss-Penzias et al., 2006). The atmospheric lifetime of gas phase elemental mercury (GEM) has been estimated to be 0.5–2 years (Schroeder and Munthe, 1998; Bergan et al., 1999; Bergan and Rodhe, 2001). More recent studies have indicated a shorter lifetime of 0.5–6 months in certain marine boundary layer environments (Weiss-Penzias et al., 2003; Hedgecock et al., 2005). It is also generally assumed that gas phase RGM should have very low concentrations in clean, background air because of rapid deposition (Landis et al., 2002) and scrubbing by clouds and raindrops.

The major oxidation pathways of atmospheric GEM are believed to be the gas phase reactions with ozone and OH, and the gas + aqueous oxidation by ozone, which takes place in fog and cloud droplets (Lin and Pehkonen, 1999; Selin et al., 2007) and to some extent in deliquesced aerosol particles (Pirrone et al., 2000). There is considerable uncertainty over the reaction rates and mechanisms for RGM production (e.g. Pal and Ariya, 2004a; Calvert and Lindberg, 2005; Holmes et al., 2006). However, global scale models suggest the prevalence of the OH oxidation over O_3, in RGM formation (Selin et al., 2007). Less is known about halogen containing compound concentrations and their variation in space and time, which makes it difficult to estimate the importance of these reactions on a global scale (Holmes et al., 2006).

Current estimates suggest that over half of the global anthropogenic atmospheric mercury emissions are from Asia, with the large majority (50% of Asian emission) coming from China (Pacyna et al., 2003; Pan et al., 2006). Out of the total Hg emissions in China, the reported breakdown by species is 56% as GEM, 32% as RGM and 12% as PHg (Streets et al., 2005). Fang et al. (2004) have shown that only 12% of the mercury emitted from coal combustion is deposited locally; the rest participated in the regional or global Hg cycle, although no details on Hg speciation were provided.

To date, few atmospheric measurements have been made to verify the large Asian emissions reported in the inventories of Wang et al. (2000); Pacyna et al. (2003) and Streets et al. (2005). In order to better interpret the nature of source regions, source types and characterization of mercury outflow from East Asia, an intensive field campaign was conducted at Cape Hedo Observatory (CHO) on the island of Okinawa, Japan. These data have been analyzed with respect to the outflow of GEM from Asia, with particular focus on comparing the GEM/CO ratio to the emission inventory (Jaffe et al., 2005). In that work we found that the total GEM export (including natural + re-emissions) exceeded the emission inventory by ~100%. This result was confirmed by the modeling studies of Pan et al. (2006) and Selin et al. (2007).

The research presented here is a further analysis of the data collected at Cape Hedo on the island of Okinawa, with an emphasis on the sources, variability and regional transport of RGM and PHg. In particular, we will focus on answering the following questions: (1) What is the magnitude of RGM and PHg during outflow from East Asia? (2) What controls the concentration of RGM and PHg? (3) What are the relationships between RGM, PHg and other compounds? (4) What characteristics of the Asian outflow events explain the observed concentration of mercury species on an event basis?

2. Instrumentation and methods

The Cape Hedo Observatory (CHO; 26.8°N, 128.2°E, 60 m amsl) is located on the north end of the island of Okinawa, away from the island's major population centers (Fig. 1). Being situated in the Pacific marine environment, downwind of the major Asian emission region, this site has unique importance for the study of atmospheric pollution. In winter (January–March), winds carry Asian (mostly Chinese) pollution and spread it over the Pacific Ocean. At Okinawa, April/May is the meteorological transition period and winds from either the east or west can be encountered. During summer and autumn seasons, winds at Okinawa are from west to east, with cleaner air from the Pacific Ocean. Thus spring (March–May) is an optimum period to study the transport of pollution from Asia to the Pacific Ocean. Due to meteorological and geographical importance, this site has been used for a number of years to study the outflow of pollution from East Asia and China (Kanaya et al., 2001; Kato et al., 2004; Takami et al., 2005).

Measurement of a variety of aerosols and trace gases was made during the spring of 2004 at CHO (Table 1). Gaseous elemental mercury (GEM), reactive gaseous mercury (RGM) and fine (<2.5 μm) particulate-bound mercury (PHg) were measured from March 23 to May 2, 2004. The slopes from the correlation of GEM, RGM and PHg with CO are used to calculate the export of RGM and PHg. Details of the CO, O_3, and GEM measurements are given in Jaffe et al. (2005), so only a brief description is given here.

An automated mercury speciation system (Tekran 2537-1130-1135) was used to determine the concentrations of GEM, RGM and PHg. The mercury fractions are collected by sequential capture, RGM is sequestered by a KCl-coated annular-denuder, and all remaining fine particulate matters are then captured on a quartz-fiber filter. GEM passes through all steps quantitatively and is pre-concentrated on alternating gold cartridges, thermally desorbed, and detected by cold vapor atomic fluorescence spectroscopy (CVAFS). The RGM and PHg fractions are quantified by thermal desorption and reduction to GEM in a mercury-free carrier gas, and then quantified as GEM. GEM analysis occurs every 5 min, whereas RGM and PHg are accumulated on the denuder/filter combination for 3 h prior to

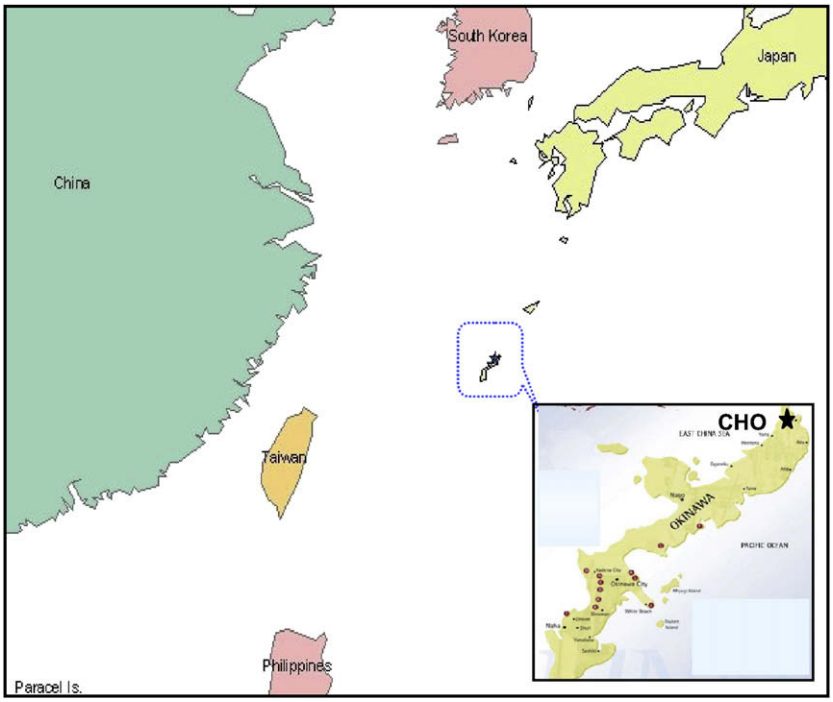

Fig. 1. Location of the Cape Hedo Observatory (CHO; 26.8°N, 128.2°E, 60 m amsl) at Okinawa, Japan. The lower right panel is a magnified picture of Okinawa Island and CHO is shown by the 'star' symbol.

analysis. A detector calibration was done every 40 h with excellent control (%RSD < 1.39% and A–B cartridge ratio of 0.998, $n = 26$). The method is described fully by Landis et al. (2002).

A Radiance Research nephelometer with an impactor having a cutoff size of 1 μm aerodynamic diameter was used to measure the light scattering coefficient by submicron aerosols (σ_{scat}). Observations of temperature (T), relative humidity (RH), wind speed (WS), wind direction (WD) and solar flux (visible) were also made to support this study. SO_2 was measured by conventional analyzer (Horiba APSA-365) based on pulsed fluorescence technology (Takami et al., 2005, 2007).

Submicron (approx. $PM_{1.0}$) aerosol species (SO_4, NH_4, NO_3, organics) were measured by an Aerodyne Quadrupole aerosol mass spectrometer (Q-AMS, Aerodyne Research Inc., MA) based on vaporization and ionization techniques. Detailed descriptions, analysis method and set-up conditions of AMS at CHO can be found elsewhere (Takami et al., 2005; Allan et al., 2003, 2004; Takami et al., 2007). Organic mass is obtained by subtracting both gaseous species and inorganic species (SO4, NH4, NO3, etc.) from total mass. The submicron aerosol mass (SAM) is the sum of the dominant aerosol species (SO4, NH4, NO3, organics) measured by Q-AMS. The aerosols sampled by Q-AMS have approximately the same cutoff size as the aerosols sampled by the nephelometer (1 μm).

CHO is located at 60 m asl in a large clearing about 100 m from the ocean. Inlets for all of the instruments at CHO were located on the roof of the instrument shelter, approximately 5 m above ground height. The surroundings within 0.5 km are mainly rocks, plowed fields or sugar cane. Due to the coastal nature of the site we expect little influence on Hg concentration from local vegetation.

Table 1
Statistical summary of the three forms of mercury and other observed parameters

Measured parameters	Data (points)	5th%	25th%	75th%	95th%	Mean	Median	SD
GEM (ng m^{-3})	686	1.54	1.79	2.21	2.71	2.04	1.99	0.38
PHg (pg m^{-3})	238	0.7	1.5	3.7	7.7	3.0	2.4	2.4
RGM (pg m^{-3})	238	0.3	0.8	5.9	16.5	4.5	2.5	5.4
RGM daytime	89	0.3	1.3	8.8	20.4	6.3	4.2	6.3
RGM nighttime	110	0.3	0.7	4.4	10.5	3.3	2.1	3.8
σ_{scat} (M m^{-1})	871	9.5	22.5	52.3	113.7	43.7	31.8	35.3
CO (ppbv)	943	143.2	173.3	240.5	324.6	214.9	199.8	65.2
O_3 (ppbv)	943	12.5	23.1	38.0	49.6	31.0	30.7	10.9
SAM (μg m^{-3})	803	1.2	3.8	8.0	20.2	7.0	5.7	5.5

Other than RGM and PHg (3 hourly point), all data are at hourly intervals. RGM daytime data are averaged from 10 am to 6 pm and nighttime data are 8 pm to 6 am.

We used the Hybrid Single-Particle Lagrangian Integrated Trajectory (HYSPLIT-4) model (Draxler and Rolph, 2003) to calculate back trajectories and obtain the hourly mixing layer height and precipitation using the FNL data set. The mixing layer height was used to detect if the air parcel was in the boundary layer or the free troposphere. Precipitation was used to assess the wet removal of mercury and other species. Since air mass transport time from the Chinese coastal region to CHO ranged from 24 h to 55 h (Uno et al., 1998), we decided to use 3-day (72 h) kinematic back trajectories initiated each hour from CHO. We also used the HYSPLIT dispersion model to evaluate the influence of wet-deposition removal on reactive mercury species and particulate mercury.

3. Results and discussion

3.1. Statistical overview

Table 1 gives a statistical summary of the key observations. All data are reported and used as hourly averages, except for RGM and PHg, which are reported as 3 h averages. Variability (95th%/5th%) of one order of magnitude is observed in the hourly concentration of RGM, PHg and aerosol species, whereas CO and GEM show lower variability (factor of 2). Fig. 2 shows a time series of GEM, CO, RGM, PHg, SO_4 and SAM. RGM shows a diurnal cycle on most days with a peak near local noon. This diurnal pattern is not observed in other species shown in plates 2b and c.

The average levels of GEM, RGM and PHg during the entire campaign period are 2.04 ± 0.38 ng m^{-3}, 4.5 ± 5.4 pg m^{-3} and 3.05 ± 2.45 pg m^{-3}, respectively (Table 1).

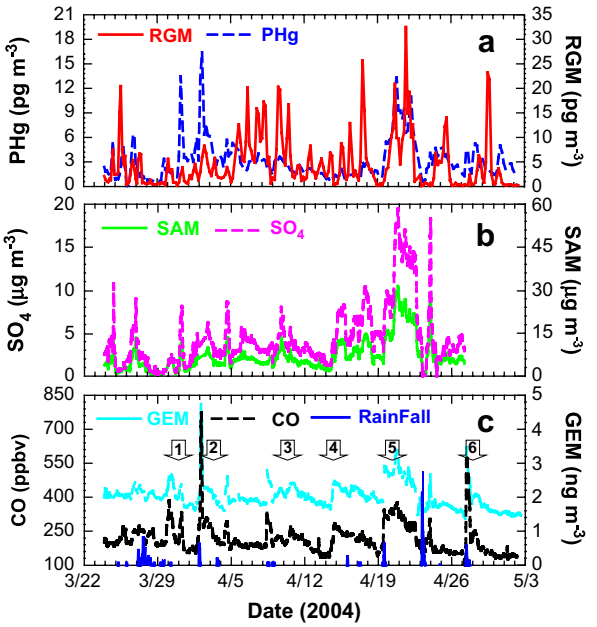

Fig. 2. Time series of (a) short-lived species RGM and PHg, (b) SO_4 and submicron aerosol mass (SAM), (c) GEM, CO and rainfall. The rainfall (arbitrary units) shown here is not from CHO but from the nearest two sites (Oku and Nago). The legends show the respective variables in each plate and the numbers in the lowest plate show the regional transport events.

Long-lived species like GEM and CO show lower variability compared to the short-lived species like RGM, PHg, SO_4 and SAM. The average temperature, relative humidity and wind speed at CHO during the campaign period are 20.3 ± 2.7 °C, $80 \pm 11\%$ and 4.44 ± 2.26 m s^{-1}, respectively. The wind shows a similar distribution in day and night without any land–sea breeze affect. Being on a small island, the range of hourly mean temperature is relatively narrow (19–22 °C), and the mixed layer height likely has only a small variation through the day. So we attribute the large variability in the gaseous and aerosol parameters mainly to horizontal transport.

Jaffe et al. (2005) identified six episodes of transported Asian pollution to the site. These events are shown (#1–6) in Fig. 2c. In the earlier analysis, we used the GEM/CO ratios during these six episodes to quantify the GEM export from Asia. In a later section of this paper we will focus on events #4 and #5 to assess the transport of RGM and PHg and to compare these species with long-lived (GEM and CO) and short-lived tracers (SAM and SO_2).

During many days, RGM shows a diurnal variation with a daytime peak lasting for 6–12 h (66% days of campaign period). Since other pollution tracers did not show this cycle, the RGM diurnal pattern is not likely due to horizontal or vertical transport of pollutants. Instead, the diurnal cycle suggests oxidation of GEM by a photochemically generated oxidant, such as OH. There are a few events, such as April 18th, when RGM and PHg show enhanced levels even during nighttime. However, on these dates other pollutants are also enhanced and this is linked to an extended multi-day pollution episode.

3.2. Correlations among key species

Table 2 shows a correlation matrix of the different gaseous and aerosol species. Significant ($p < 0.05$) correlations are observed among all species except CO-RGM. The best correlations are observed between CO and GEM

Table 2
Matrix of correlations with first row and column showing the observed species

	GEM	PHg	RGM	σ_{scat}	CO	O_3
PHg	0.49	1				
	<0.01	–				
	238	238				
RGM	0.2	0.32	1			
	<0.01	<0.01	–			
	238	238	238			
σ_{scat}	0.71	0.74	0.34	1		
	<0.01	<0.01	<0.01	–		
	628	219	219	869		
CO	0.92	0.5	0.12	0.68	1	
	<0.01	<0.01	<0.06	<0.01	–	
	684	238	238	869	943	
O3	0.32	0.46	0.15	0.43	0.28	1
	<0.01	<0.01	<0.02	<0.01	<0.01	–
	683	237	237	868	943	943
SAM	0.65	0.58	0.43	0.94	0.59	0.52
	<0.01	<0.01	<0.01	<0.01	<0.01	<0.01
	580	203	203	729	802	802

The 1st, 2nd and 3rd numbers in each cell are the Pearson correlation coefficient (R), significance (two-tailed) and numbers of data points, respectively.

($R = 0.92$), and SAM and σ_{scat} ($R = 0.94$). PHg shows a moderate correlation with SAM and σ_{scat}. In general, the correlations are stronger among the species having similar removal mechanisms and lifetimes (e.g. CO to GEM and SAM to PHg).

The aerosol mass and particulate mercury show a moderate degree of correlation with a slope (ΔPHg/ΔSAM) of 0.20 $\mu g\,g^{-1}$ ($R = 0.58$, $p < 0.01$). Since PHg sampling has a higher cutoff than the SAM (2.5 μm vs 1.0 μm), this ratio may be an upper limit of the actual value. By using a dry aerosol light scattering efficiency of 3 $m^2\,g^{-1}$, we find a very similar correlation and slope if we use the PHg–σ_{scat} relationship instead. The standard error on the slope ΔPHg/ΔSAM is 0.012 (i.e. 6%). This relationship shows that during outflow events, the Hg fraction of the submicron aerosol mass is relatively consistent. The Hg fraction of the fine aerosol mass observed here is much smaller than that observed by Xiu et al. (2005) in Shanghai. Using a different methodology, Xiu et al. (2005) found Hg particulate mass fraction of the fine mode aerosol of 3–4 $\mu g\,g^{-1}$. Their method was to collect fine PM on high volume filters, followed by laboratory analysis of the collected Hg. While the total PM mass certainly decreases during transport to Okinawa, it is likely that the PHg fraction would increase if RGM is produced and adsorbed onto pre-existing aerosols. On the other hand, it is also possible that mercury adsorbed on the particulate matter could be released by both thermal and incident radiations during transport, as discussed by Gustin et al. (2002). The time of year between Xiu et al. (2005) and this study could also be important to explain some of the differences. However, we believe the most likely cause for the difference between our result and that of Xiu et al. (2005) is due to different experimental methods, since RGM will collect on the filters and can result in a significant positive artifact (Landis et al., 2002; Lyman and Keeler, 2002). We believe our measured slope (ΔPHg/ΔSAM) is an accurate representation of the Hg content of fine aerosols leaving the Asian continent.

Table 3 shows the correlations of three mercury species with CO during the six pollution episodes observed during the campaign (see Fig. 2). For each event, we calculate the fraction of total Hg that is exported as PHg and RGM from the slope of the correlation of each species with CO. Out of these six transport events, event #5 (April 20–25) shows the highest export of PHg, RGM and GEM showing peak values $\sim$22 pg m^{-3}, $\sim$32 pg m^{-3} and $\sim$1.5 ng m^{-3}, respectively. However, even during event #5 RGM + PHg export is only 1.2% of GEM. In contrast, event #4 shows minimal enhancements in both RGM and PHg (Fig. 2). The average combined export for RGM + PHg for these six events is less than 1% of GEM.

In an emission mapping study, Pacyna and Pacyna (2002) and Pacyna et al. (2003) reported that 56% ($\sim$1071 ton) of global anthropogenic mercury emissions are from Asia, and nearly half of this mercury in Asia is emitted in the form of RGM and PHg. In a similar study covering 32 provinces in China, Streets et al. (2005) reported that about 44% (237 ton) of the mercury is in the form of RGM and PHg. Considering our observation of low levels of RGM and PHg during Asian outflow periods, we speculate that most of the PHg and RGM that is emitted into the boundary layer is deposited near the source region, and not available for long-range transport. The other possibility is that RGM may have been reduced to GEM before it arrived at CHO. Substantial conversion of RGM into GEM is reported in downwind plumes by Lohman et al. (2006). In contrast, Friedli et al. (2004) found greater export of particulate mercury from Asia in the free troposphere. This could be due to a different observational method or greater precipitation scavenging and removal at ocean surface, compared to the free troposphere.

Fig. 3 shows the correlation of CO with GEM, SAM and SO_2 for the two consecutive events #4 and #5 ($p < 0.001$). The slopes (ΔSAM/ΔCO) for these consecutive events are 0.046 $\mu g\,m^{-3}$ $ppbv^{-1}$ and 0.120 $\mu g\,m^{-3}$ $ppbv^{-1}$. For both these events, the ΔGEM/ΔCO slopes are 5.3E-3 ng m^{-3} $ppbv^{-1}$ and 7.2E-3 ng m^{-3} $ppbv^{-1}$, respectively. Weak correlations are found between CO and SO_2 for events #4 and #5, however, correlation coefficient (R) is better for event #5 compared to event #4. The slopes and correlation coefficients of SAM/CO, GEM/CO and SO_2/CO are lower for event #4 compared to event #5. The highest export of RGM + PHg is observed in event #5. While GEM and CO are strongly enhanced in event #4, RGM and PHg show much lower concentrations during event #4 compared to event #5.

Since event #4 had less aerosol mass and PHg per unit of CO compared to event #5, we wish to identify the cause. Back trajectories indicate that during event #4 the air was aged and transported mainly within the mixing layer from southern Japan, whereas during event #5 the air parcel descended over China and picked up pollution in the boundary layer (Fig. 4). Analysis of the HYSPLIT trajectories shows that 28% and 24% of the total time the air experienced rainfall during event #4 and #5, respectively. A dramatic decrease in RGM, PHg, SO_4 and aerosol mass (SAM) was recorded during the heavy rain observed in the vicinity of CHO on April 23 (Fig. 2c). Of the total time, the air parcels resided in the mixing layer for 99% of the time during event #4 and 73% of time during event #5. We

Table 3
Summary of RGM and PHg exports (% of GEM) during six transport events at CHO

Event #	GEM vs CO Ψ1	R	PHg vs CO Ψ2	R	RGM vs CO Ψ3	R	% PHg export[a]	%RGM export[b]
Ev 1	0.0043	0.93	0.0067	0.14	0.0171	0.74	0.16	0.40
Ev 2	0.0056	0.99	0.0183	0.65	0.0011	0.10	0.33	0.02
Ev 3	0.0073	0.99	−0.0054	0.33	−0.0762	0.51	−0.07	−1.04
Ev 4	0.0051	0.88	0.0031	0.37	−0.0083	0.10	0.06	−0.16
Ev 5	0.0074	0.95	0.0436	0.77	0.0480	0.37	0.59	0.65
Ev 6	0.0036	0.96	0.0055	0.52	−0.0066	0.40	0.15	−0.18
Mean	0.0056	–	0.0120	–	−0.0042	–	0.20	−0.05
SD	0.0016	–	0.0173	–	0.0410	–	0.23	0.59
Min	0.0036	0.88	−0.0054	0.14	−0.0762	0.10	−0.07	−1.04
Max	0.0074	0.99	0.0436	0.77	0.0480	0.74	0.59	0.65

Slopes from the correlation of GEM, RGM and PHg with CO and their Pearson correlation coefficient (R) are used to calculate export of RGM and PHg.
Units: GEM (ng m^{-3}); CO (ppbv); PHg (pg m^{-3}); RGM (pg m^{-3}).
[a] Percent of total Hg exported as PHg calculated using slopes Ψ1 and Ψ2.
[b] Percent of total Hg exported as RGM calculated using slopes Ψ1 and Ψ3.

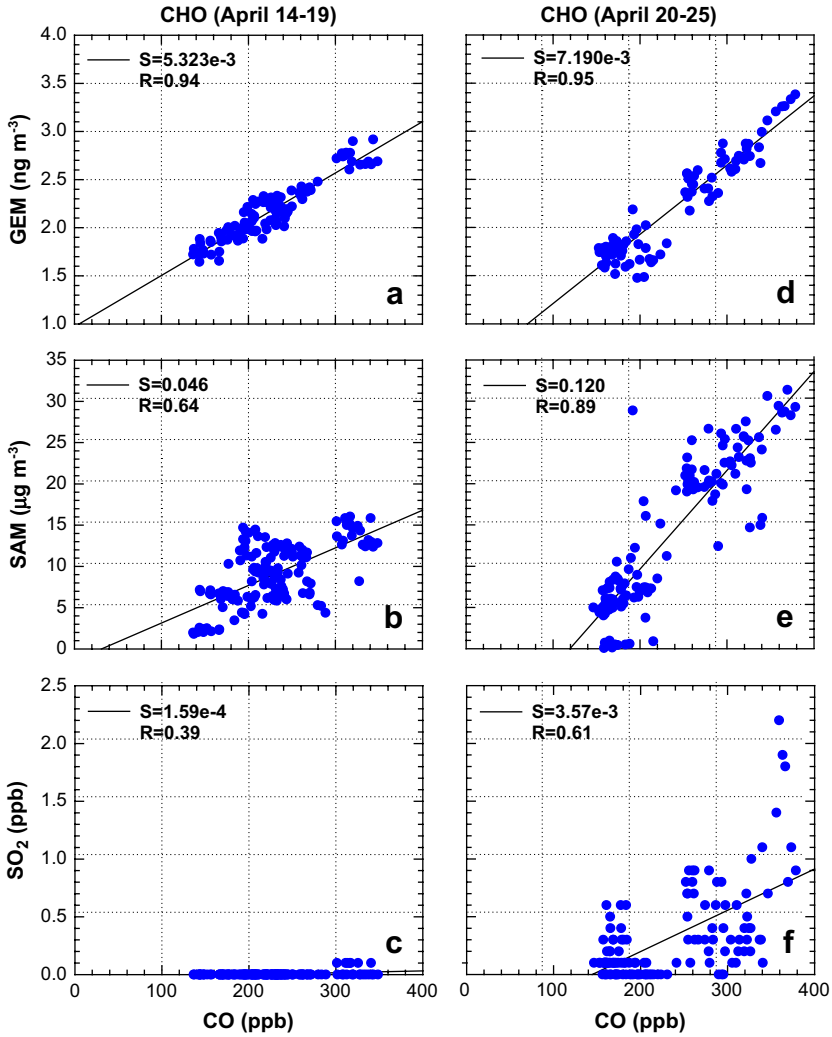

Fig. 3. Correlations in (a) CO and GEM, (b) CO and SAM, (c) CO and SO_2 for the period April 14–19, 2004; (d) CO and GEM, and (e) CO and SAM, (f) CO and SO_2 for the period April 20–25, 2004. The slope and *R* are shown for each relationship.

believe the longer residence of air in the mixed layer during event #4 which likely led to greater loss of RGM and PHg by both wet (rain) and dry depositions. Assuming a short life of SO_2 (<3 days), the low concentration as well as correlation of SO_2 with CO in event #4 further supports our argument.

We used the HYSLIT dispersion model to further evaluate the influence of wet removal on reactive mercury species and particulate mercury for events #4 and #5. For event #4, the source region was assumed to be 34.00°N 131.00°E (Southern Japan) and a release start time of 00Z April 14, 2004, was used. The release height was between 10 m and 1000 m, based on the arrival of back trajectories to CHO. For event #5, the source region was assumed to be 26.00°N 120.00°E (East China) and a release start time of 18Z April 17, 2004, was used. For both events #4 and #5, we conducted the dispersion runs with and without wet deposition. The in-cloud removal was set by the ratio of the concentration in air ($g\,l^{-1}$) to that in rain ($g\,l^{-1}$). For this ratio we used the default value for the HYSPLIT dispersion model, 3.2E5. For below-cloud scavenging, we used a removal time constant of 5.0E-5 s.

Figs. S1–S4 in the Supplementary material show animated images of the dispersion model results. For event #5, the difference between the runs with and without wet deposition was minimal. While the trajectories suggest some precipitation during transport, the deposition model results are consistent with much of the transport having occurred above the boundary layer, and thus more RGM and PHg survived transport to CHO. For event #4 this is not the case. The run with wet deposition turned off in the model has several times the concentrations compared to the model runs with wet deposition on. This indicates that wet removal was, at least in part, responsible for the much lower concentrations of RGM and PHg. It is also possible that higher particulate loadings from China, as compared to Japan, played a role.

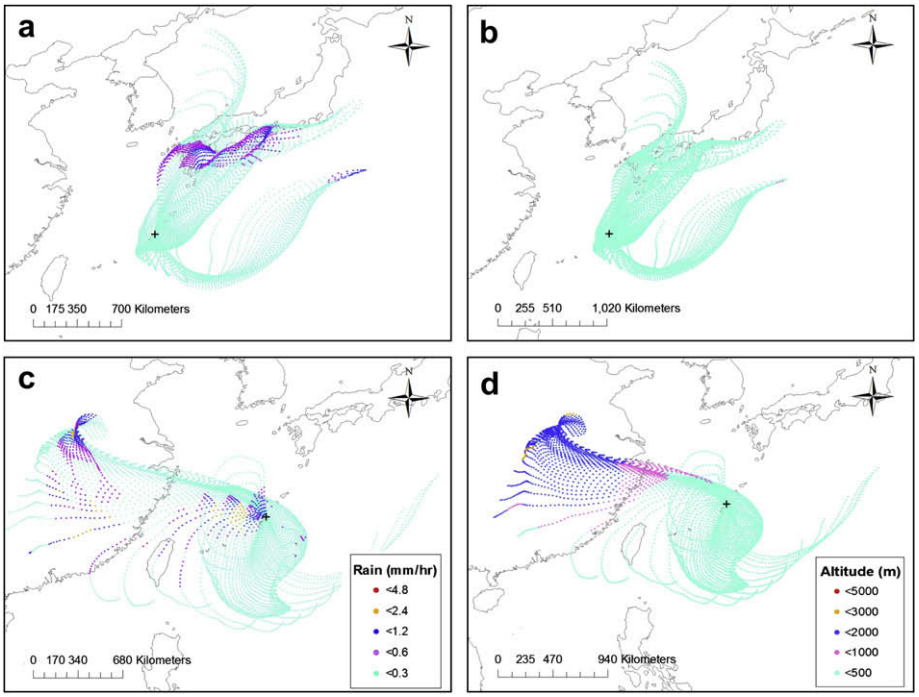

Fig. 4. NOAA-HYSPLIT 3 days back trajectories showing the history of rainfall and 3D movement of air masses for the two periods, April 14–19 (a, b, event #4) and April 20–25 (c, d event #5), respectively. For each event, we have calculated trajectories at 1-h intervals (120 trajectories). The rainfall and altitude of air parcels are shown by different colors. The arrival point of trajectories at CHO (26.8°N, 128.2°E, 60 m) is shown by the cross symbol.

3.3. Diurnal variations in RGM

Table 1 shows the statistical summary of day and nighttime RGM levels. Unlike GEM and PHg, RGM shows a diurnal variation with higher values observed in the afternoon hours. After the peak level, RGM decreases to very low levels on most days. Fig. 5 shows the diurnal variations of RGM and solar flux for the April 12–19 period. While RGM shows a diurnal variation with high concentration in the daytime and very low concentration at night (66% days of the campaign period), the correlation coefficient of RGM with solar flux is not large ($R < 0.36$, $p < 0.001$). The periods of highest solar flux (April 12 and 18) do not lead to the highest levels of RGM. There are some periods (e.g. April 14 and 18) with elevated concentrations of RGM at night. In the absence of any photochemistry, the elevated RGM at night is likely a result of horizontal transport. RGM is inversely related to wind speed and RH, however, the relationship is not strong ($R < 0.37$, $p < 0.01$). The diurnal cycle is likely driven by RGM production in daytime. Ignoring the loss term, we can estimate the production rate from the change in RGM concentration with time. For the whole campaign, the average change in RGM is 1.4 ± 1.5 pg m^{-3} h^{-1} from 8 am to 12 pm local time.

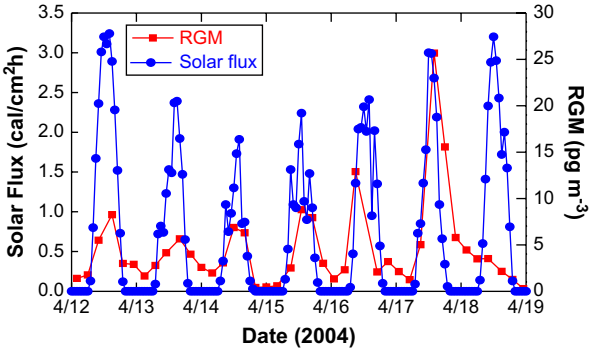

Fig. 5. Time series of the RGM and solar flux showing diurnal variation from April 12 to April 19, 2005. The time is local solar time.

RGM production is believed to primarily occur via either O_3 or OH oxidation of GEM (Pal and Ariya, 2004a; Selin et al., 2007; Hall, 1995; P'yankov, 1949; Biswajit and Parisa, 2003; Pal and Ariya, 2004b). While there is considerable uncertainty over the reaction rates and mechanisms, for both OH and O_3 (e.g. Calvert and Lindberg, 2005), one model suggests the prevalence of OH oxidation over O_3 oxidation, at least on a global scale (Selin et al., 2007). At Okinawa, the diurnal cycle in RGM suggests a diurnal production mechanism, e.g. OH oxidation, rather than O_3 oxidation. Using a rate constant of 9×10^{-14} cm^3 molecule^{-1} s^{-1} for the OH oxidation rate (Sommar et al., 2001; Pal and Ariya, 2004a) and an OH concentration of $1–5 \times 10^6$ cm^{-3} (Kanaya et al., 2001), which are typical values for the daytime marine boundary layer in spring-early summer, we find RGM production rates of 0.6–3.0 pg m^{-3} molecule^{-1} h^{-1}. This is consistent with the observed daytime increase in RGM concentration of 1.4 ± 1.5 pg m^{-3} h^{-1} between 8 h and 12 h (local time). It should be noted here that this is the average value, and the difference in the calculated and

observed RGM is highly variable on a day-to-day basis. This day-to-day variation may be due to varying loss by deposition and chemistry, changing concentrations of precursors, perturbation in large scale meteorology and the presence of other chemical parameters (e.g. aerosols, halogen and other chemical species) (Lin et al., 2006). While these data are consistent with an OH oxidation mechanism, this does not preclude other mechanisms from also being important, e.g. Br oxidation (Holmes et al., 2006). This is especially important to stress given the large uncertainties in the O_3 and OH oxidation rates (Calvert and Lindberg, 2005).

4. Conclusions

During March 23 to May 2, 2004, speciated mercury (GEM, PHg, RGM) was measured at Cape Hedo Observatory at Okinawa Island (Japan), downwind of the major Asian source regions. Here we focus on reactive and particulate mercury transports from Asia and their possible link with other atmospheric trace species and meteorological conditions over the western Pacific. Large variability is observed in the pollutant air species at CHO. The mean and 1σ concentrations of gaseous elemental mercury (GEM), reactive gaseous mercury (RGM) and particulate-bound mercury (PHg) were found to be $2.04 \pm 0.38\ \mathrm{ng\,m^{-3}}$, $4.5 \pm 5.4\ \mathrm{pg\,m^{-3}}$ and $3.0 \pm 2.5\ \mathrm{pg\,m^{-3}}$, respectively. The combined export of RGM and PHg is less than 1% of the total Hg. This indicates that most of the atmospheric mercury exported from Asia is in the form of GEM and outflow of RGM and PHg in the East Asian boundary layer is minimal. However, this does not preclude export of these species at higher elevations.

During outflow events, we found a mean PHg/SAM ratio of $0.20 \pm 6\%\ \mu\mathrm{g\,g^{-1}}$, which we believe to be characteristic of East Asian industrial aerosols during outflow. Lower ratios of SAM/CO and GEM/CO in events of rain and air parcels residing in the mixing layer indicate that meteorology plays an important role in the lifetimes of RGM, SAM and other aerosols species. Unlike GEM and PHg, RGM shows a diurnal variation with a peak near local noon. A first-order estimate suggests that the diurnal variability of RGM can be explained by OH chemistry. However, halogens or other oxidants could also be important. To better understand the atmospheric budget, lifetime and transport of all three species of mercury in the marine boundary layer, comprehensive measurements of different forms of mercury along with OH and major halogen species are needed near source regions and their downwind sites in the boundary layer as well as the free troposphere.

Acknowledgements

The research presented in this article was primarily funded by the U.S. Environmental Protection Agency's STAR program, with additional support from the Electric Power Research Institute (EPRI). The results have not been subjected to any EPA review and, therefore, do not necessarily reflect the views of the Agency. We acknowledge the anonymous reviewer for meticulously going through our MS and his/her constructive comments.

Appendix. Supplementary material

Supplementary data associated with this article can be found in the online version, at 10.1016/j.atmosenv.2008.06.048.

References

Allan, J.D., Jimenez, J.L., Coe, H., Bower, K.N., Williams, P.I., Worsnop, D.R., 2003. Quantitative sampling using an Aerodyne aerosol mass spectrometer, Part 1: techniques of data interpretation and error analysis. Journal of Geophysical Research 108 (D3), 4090. doi:10.1029/2002JD002358.

Allan, J.D., Delia, A.E., Coe, H., Bower, K.N., Rami Alfarra, M., Jimenez, J.L., Middlebrook, A.M., Drewnick, F., Onasch, T.B., Canagaratna, M.R., Jayne, J.T., Worsnop, D.R., 2004. Technical note: extraction of chemically resolved mass spectra from Aerodyne aerosol mass spectrometer data. Journal of Aerosol Science 35, 909–922.

Bergan, T., Gallardo, L., Rodhe, H., 1999. Mercury in the global troposphere: a three dimensional model study. Atmospheric Environment 33, 1575–1585.

Bergan, T., Rodhe, H., 2001. Oxidation of elemental mercury in the atmosphere: constraint imposed by global scale modeling. Journal of Atmospheric Chemistry 40, 192–212.

Biswajit, P., Parisa, A.A., 2003. Atmospheric reactions of gaseous mercury with ozone and hydroxyl radical: kinetics and product studies. Journal de Physique, IV 107 (Part 1), 189–192.

Calvert, J.G., Lindberg, S.E., 2005. Mechanisms of mercury removal by O_3 and OH in the atmosphere. Atmospheric Environment 39 (18), 3355–3367.

Carpi, A., 1997. Mercury from combustion sources: a review of the chemical species emitted and their transport in the atmosphere. Water, Air, and Soil Pollution 98, 241–254.

Draxler, R.R., Rolph, G.D., 2003. HYSPLIT (HYbrid Single-Particle Lagrangian Integrated Trajectory). NOAA Air Resources Laboratory, Silver Spring, MD. Model access via NOAA ARL READY Website: http://www.arl.noaa.gov/ready/hysplit4.html.

Fang, F.M., Wang, W., Li, J., 2004. Urban environmental mercury in Changchun, a metropolitan city in Northeastern China: source, cycle, and fate. Science of the Total Environment 330, 159–170.

Friedli, H.R., Radke, L.F., Prescott, R., Li, P., Woo, J.-H., Carmichael, G.R., 2004. Mercury in the atmosphere around Japan, Korea, and China as observed during the 2001 ACE-Asia field campaign: measurements, distributions, sources, and implications. Journal of Geophysical Research 109, D19S25. doi:10.1029/2003JD004244.

Gustin, M.S., Biester, H., Kim, C.S., 2002. Investigation of the light-enhanced emission of mercury from naturally enriched substrates. Atmospheric Environment 36, 3241–3254.

Hall, B., 1995. The gas-phase oxidation of elemental mercury by ozone. Water, Air, and Soil Pollution 80 (1–4), 301–315.

Hedgecock, I.M., Trunfio, G.A., Pirrone, N., Sprovieri, F., 2005. Mercury chemistry in the MBL: Mediterranean case and sensitivity studies using the AMCOTS (Atmospheric Mercury Chemistry over the Sea) model. Atmospheric Environment 39, 7217–7230.

Holmes, C.D., Jacob, D.J., Yang, X., 2006. Global lifetime of elemental mercury against oxidation by atomic bromine in the free troposphere. Geophysical Research Letters 33 (20), L20808.

Jaffe, D.A., Prestbo, E., Swartzendruber, P., Weiss-Penzias, P., Kato, S., Takami, A., Hatakeyama, S., Kajii, Y., 2005. Export of atmospheric mercury from Asia. Atmospheric Environment 39, 3029–3038.

Kanaya, Y., Sadanaga, Y., Nakamura, K., Akimoto, H., 2001. Behavior of OH and HO_2 radicals during the observations at a remote Island of Okinawa (ORION99) field campaign 1. Observation during a laser induced fluorescence instrument. Journal of Geophysical Research 106 (D20), 24197–24208.

Kato, S., Kajii, Y., Itokazu, R., Hirokawa, J., Koda, S., Kinjo, Y., 2004. Transport of atmospheric carbon monoxide, ozone, and hydrocarbons from Chinese coast to Okinawa Island in the Western Pacific during winter. Atmospheric Environment 38 (19), 2975–2981.

Landis, M.S., Stevens, R.K., Schaedlich, F., Prestbo, E.M., 2002. Development and characterization of an annular denuder methodology for the measurement of divalent inorganic reactive mercury in the ambient air. Environmental Science and Technology 36, 3000–3009.

Lin, C.J., Pehkonen, S.O., 1999. The chemistry of atmospheric mercury: a review. Atmospheric Environment 33, 2067–2079.

Lin, C.J., Pongprueksa, P., Lindberg, S.E., Pehkonen, S.O., Byun, D., Jang, C., 2006. Scientific uncertainties in atmospheric mercury models I:

model science evaluation. Atmospheric Environment 40 (16), 2911–2928.
Lipfert, F., Morris, S., Sullivan, T., Moskowitz, P., Renninger, S., 2005. Methylmercury, fish consumption, and the precautionary principle. Journal of Air and Waste Management Association 55, 388–398.
Lohman, K., Seigneur, C., Edgerton, E., Jansen, J., 2006. Modeling mercury in power plant plumes. Environmental Science and Technology 40, 3848–3854.
Lyman, M.M., Keeler, G.J., 2002. Comparison methods for particulate phase mercury analysis: techniques and sampling artifacts. Fresnius Journal of Analytical Chemistry 374, 1009–1014.
P'yankov, V.A., 1949. Russian Journal of General Chemistry 19, 224–229.
Pacyna, E.G., Pacyna, J.M., 2002. Global emission of mercury from anthropogenic sources in 1995. Water, Air and Soil Pollution 137 (1–4), 149–165.
Pacyna, J.M., Pacyna, E.G., Steenhuisen, F., Wilson, S., 2003. Mapping 1995 global anthropogenic emissions of mercury. Atmospheric Environment 37 (S1), 109–117.
Pal, B., Ariya, P.A., 2004a. Gas-phase HO center dot-initiated reactions of elemental mercury: kinetics, product studies, and atmospheric implications. Environmental Science and Technology 38 (21), 5555–5566.
Pal, B., Ariya, P.A., 2004b. Studies of ozone initiated reactions of gaseous mercury: kinetics, product studies, and atmospheric implications. Physical Chemistry Chemical Physics 6 (3), 572–579.
Pan, L., Woo, J.-H., Carmichael, G.R., Tang, Y., Friedli, H.R., Radke, L.F., 2006. Regional distribution and emissions of mercury in East Asia: a modeling analysis of Asian Pacific Regional Aerosol Characterization Experiment (ACE-Asia) observations. Journal of Geophysical Research 111, D07109. doi:10.1029/2005JD006381.
Pirrone, N., Hedgecock, I., Forlano, L., 2000. The role of the ambient aerosol in the atmospheric processing of semi-volatile contaminants: a parameterized numerical model (GASPAR). Journal of Geophysical Research 105 (D8), 9773–9790.
Schroeder, W.H., Munthe, J., 1998. Atmospheric mercury: an overview. Atmospheric Environment 32, 809–822.
Selin, N.E., Jacob, D.J., Park, R.J., Yantosca, R.M., Strode, S., Jaeglé, L., Jaffe, D. , 2007. Chemical cycling and deposition of atmospheric mercury: global constraints from observations. Journal of Geophysical Research 112 (D2), D02308.
Sommar, J., Gardfeldt, K., Stromberg, D., Feng, X., 2001. A kinetic study of the gas phase reaction between the hydroxyl radical and atomic mercury. Atmospheric Environment 35, 3049–3054.
Streets, D.G., Hao, J., Wu, Y., Jiang, J., Chan, M., Tian, H., Feng, X., 2005. Anthropogenic mercury emissions in China. Atmospheric Environment 39, 7789–7806.
Takami, A., Miyoshi, T., Shimono, A., Hatakeyama, S., 2005. Chemical composition of fine aerosol measured by AMS at Fukue Island, Japan during APEX period. Atmospheric Environment 39, 4913–4924. doi:10.1016/j.atmosenv.2005.04.038.
Takami, A., Miyoshi, T., Shimono, A., Kaneyasu, N., Kato, S., Kajii, Y., Hatakeyama, S., 2007. Transport of anthropogenic aerosols from Asia and subsequent chemical transformation. Journal of Geophysical Research. doi:10.1029/2006JD008120.
Uno, I., Ohara, T., Murano, K., 1998. Simulated acidic aerosol long-range transport and deposition over East Asia – role of synoptic scale weather systems. In: Gryning, S.-E., Chaumerliac, N. (Eds.), Air Pollution Modeling and its Application XII. Plenum Press, New York.
Wang, Q., Shen, W.G., Ma, Z.W., 2000. Estimation of mercury emissions from coal combustion in China. Environmental Science and Technology 34 (13), 2711–2713.
Weiss-Penzias, P., Jaffe, D.A., McClintick, A., Prestbo, E.M., Landis, M.S., 2003. Gaseous elemental mercury in the marine boundary layer: evidence for rapid removal in anthropogenic pollution. Environmental Science and Technology 37 (17), 3755–3763.
Weiss-Penzias, P., Jaffe, D.A., Swartzendruber, P., Dennison, J.B., Chand, D., Hafner, W., Prestbo, E., 2006. Observations of Asian air pollution in the free troposphere at Mount Bachelor Observatory during the spring of 2004. Journal of Geophysical Research 111, D10304. doi:10.1029/2005JD006522.
Xiu, G.L., Jin, Q., Zhang, D., Shi, S., Huang, X., Zhang, W., Bao, L., Gao, P., Chen, B., 2005. Characterization of size-fractionated particulate mercury in Shanghai ambient air. Atmospheric Environment 39 (3), 419–427.